Active Site Structure of Methylamine Dehydrogenase: Hydrazines Identify C6 as the Reactive Site of the Tryptophan-Derived Quinone Cofactor[†,‡]

Eric. G. Huizinga,[§] Ben A. M. van Zanten,[§] Johannis A. Duine,[∥] Jaap A. Jongejan,[∥] Fienke Huitema,[∥] Keith S. Wilson,[⊥] and Wim G. J. Hol[*,§]

BIOSON Research Institute, Department of Chemistry, Groningen University, Nyenborgh 4, 9747 AG Groningen, The Netherlands, Department of Microbiology and Enzymology, Delft University of Technology, Julianalaan 67, 2628 BC Delft, The Netherlands, and EMBL Outstation, Notkestrasse 85, 2000 Hamburg, Germany

Received April 21, 1992; Revised Manuscript Received July 27, 1992

ABSTRACT: To identify the reactive part of the orthoquinone function of the tryptophan-derived cofactor found in methylamine dehydrogenase (MADH), we have determined the crystal structures of MADH from *Thiobacillus versutus* inhibited by methylhydrazine and (2,2,2-trifluoroethyl)hydrazine. Extra electron density attached to C6 of the tryptophyl tryptophanquinone cofactor shows that this atom and not C7 is the reactive part of the *ortho*-quinone moiety. The density retained after hydrazine inhibition is much less extensive than expected, however, suggesting that partial breakdown of the inhibitors after reaction with the cofactor may take place. A detailed description is presented of the cofactor environment in an improved model of MADH which now includes information from the recently determined gene sequence of the cofactor-containing subunit [Ubbink, M., van Kleef, M. A. G., Kleinjan, D., Hoitink, C. W. G., Huitema, F., Beintema, J. J., Duine, J. A., & Canters, G. W. (1991) *Eur. J. Biochem. 202*, 1003–1012]. We hypothesize that Asp76 is responsible for proton abstraction from the α-carbon of the substrate during catalysis.

Methylamine dehydrogenase (MADH,[1] EC 1.4.99.3) is induced in several strains of Gram negative methylotrophic bacteria when these are grown on methylamine. The enzyme isolated from *Thiobacillus versutus*, which is used in our studies, is very similar to MADH's isolated from other sources. The enzyme catalyzes the oxidative deamination of primary amines to the corresponding aldehydes plus ammonia and transfers electrons to a *c*-type cytochrome (Lommen et al., 1990) via a mediating blue copper protein named amicyanin (Houwelingen et al., 1985). MADH from *T. versutus* has a tetrameric structure consisting of two identical heavy (H) and two identical light (L) subunits with molecular masses of 47.5 (Vellieux et al., 1986) and 12.9 kDa (Ubbink et al., 1991), respectively.

The identity of the redox cofactor of MADH has been the subject of intense investigations. Until recently, MADH was thought to contain pyrroloquinoline quinone (PQQ) (de Beer et al., 1980; van de Meer et al., 1987), covalently attached at two positions to each of the L subunits (Ishii et al., 1983). The 2.25-Å X-ray structure of MADH from *T. versutus* showed, however, that the electron density in the active site region was not in accordance with a PQQ cofactor as such (Vellieux et al., 1989). When the determination of the gene sequence of the L subunit of MADH from *Methylobacterium extorquens* finally allowed identification of both residues thought to be responsible for binding the cofactor, these proved to be tryptophans (Chistoserdov et al., 1990). Combining this information with results of NMR and mass spectroscopy, McIntyre et al. (1991a) proposed that the prosthetic group of MADH actually is tryptophyl tryptophanquinone (TTQ, Figure 1). TTQ is made up of two tryptophan residues from the L subunit covalently linked through a C2′–C4 bond; one of the tryptophans is oxidized to indole-6,7-dione. At present, nothing is known about the biochemistry of cofactor formation. Supporting evidence for the TTQ cofactor model comes from X-ray studies in which it was shown that TTQ can be accommodated neatly in the active site electron densities of both MADH from *T. versutus* and from *Paracoccus denitrificans* (Chen et al., 1991). Resonance Raman studies of MADH from *P. denitrificans* and *T. versutus* (Backes et al., 1991) and MADH from *bacterium W3A1* (McIntyre et al., 1991b) strongly suggest that the same cofactor is present in all three proteins.

MADH is inactivated by many compounds known to react with carbonyl groups, showing that the quinone function is involved in catalysis (Eady & Large, 1971; Kenney & McIntyre, 1983). The structure of the TTQ cofactor raises a prominent question: at which carbon atom of the quinone function, C6 or C7, does the catalytic reaction take place? To answer this question, we have made use of hydrazines, irreversible inhibitors of MADH, which react with the cofactor and are thought to yield a product which could either be the azo- or hydrazo- adduct (Figure 2; van der Meer et al., 1987). Actually the previous identification of the cofactor as PQQ was based upon analysis of a phenylhydrazine adduct of the isolated putative cofactor (van der Meer et al., 1987), but it is now clear that this identification method is nonspecific (Klinman, 1991). In this paper, we present the crystal structures of MADH from *T. versutus* after reaction with methyl- and (trifluoroethyl)hydrazine.

These structures, together with an improved model for native MADH obtained after incorporation of the recently determined sequence of the L subunit (Ubbink et al., 1991), give

[†] This research was supported by the Netherlands Foundation for Chemical Research (SON) with financial aid from the Netherlands Organization for Scientific Research (NWO).

[‡] The atomic coordinates of the structures described in this article have been deposited in the Protein Data Bank. The file names are 2MAD (native MADH), 1MAE (MADH inhibited with methylhydrazine), and 1MAF [MADH inhibited with (trifluoroethyl)hydrazine].

[*] To whom correspondence should be addressed.

[§] BIOSON Research Institute Groningen.

[∥] Delft University of Technology.

[⊥] EMBL outstation Hamburg.

[1] Abbreviations: MADH, methylamine dehydrogenase; PQQ, pyrroloquinoline quinone; TTQ, tryptophyl tryptophanquinone; TFEH, (2,2,2-trifluoroethyl)hydrazine; MH, methylhydrazine.

0006-2960/92/0431-9789$03.00/0

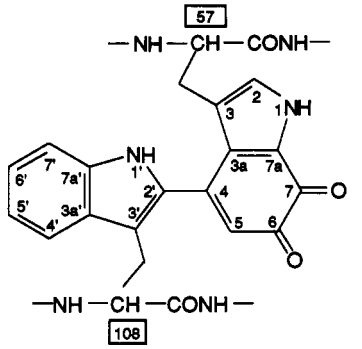

FIGURE 1: Tryptophyl tryptophanquinone cofactor of MADH. The precursor tryptophans are at positions 57 and 108 in the amino acid sequence as derived from the gene sequence of *T. versutus* MADH (Ubbink et al., 1991). To reflect this fact, the two moieties forming the cofactor in the mature enzyme are referred to as Trq57 and Trp'108 in the text.

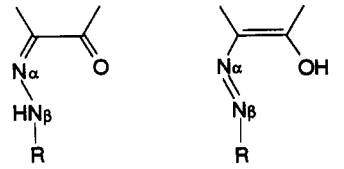

FIGURE 2: Anticipated adducts of hydrazines with the orthoquinone function of the TTQ cofactor. R = CH_3 or R = CH_2CF_3 are expected in case of inhibition with methylhydrazine (MH) and (trifluoroethyl)-hydrazine (TFEH), respectively.

a more accurate view of the cofactor environment, enabling the identification of residues making up the active site pocket and residues of possible importance for catalysis.

MATERIALS AND METHODS

(2,2,2-Trifluoroethyl)hydrazine (TFEH) and methylhydrazine (MH) were purchased from Sigma. Wurster's blue, the perchlorate salt of the cationic free radical of *N,N,N',N'*-tetramethyl-1,4-phenylenediamine, was synthesized according to Michaelis and Granich (1943). MADH was purified as described by Vellieux et al. (1986). Protein concentrations were calculated using A_{280} (1 mg/mL) = 1.14 (Vellieux et al., 1986). Absorbance spectra were recorded with a Kontron Uvicon 930 spectrophotometer.

Crystals of MH-inhibited MADH were obtained through soaking of crystals of the native protein. MADH was crystallized by the hanging drop method from 42% saturated ammonium sulfate in a 0.1 M sodium acetate buffer, pH 5.0, at 4 °C. (Vellieux et al., 1986). After reduction of the TTQ cofactor by substrate, MADH is protected from inactivation by hydrazines. In order to get complete inhibition, any reduced protein that may be present in the crystal was oxidized by Wurster's blue, an efficient artificial electron acceptor for MADH, prior to addition of hydrazine. Crystals were soaked in 2 mL of precipitant solution containing 100 μM Wurster's blue for 36 h, followed by a 24-h soak in precipitant solution containing 300 μM MH.

Crystals of TFEH inhibited MADH were obtained by inhibiting the protein prior to crystallization. To 60 μL of protein solution containing 13.3 mg/mL MADH (6.4 nmol) in 0.1 M sodium acetate buffer, pH 5.0, 10 μL of a 4.3 mM Wurster's blue solution (43 nmol) was added. After 30 min, 10 μL of a 20 mM TFEH solution (200 nmol) was added. Subsequently, the protein solution was dialyzed extensively against buffer. Enzyme activity was assayed spectrophotometrically by following the decrease in absorbance of Wurster's blue at 610 nm (Vellieux et al., 1986). Crystals were grown under the same conditions as used for native MADH, with the exception that they could only be obtained after transfer of the experiments to room temperature. Occasionally, this is also necessary for native MADH.

Table I

(a) Data Collection Parameters

	TFEH		MH	
resolution (Å)[a]	high (2.6)	low (4.5)	high (2.3)	low (3.4)
wavelength (Å)	1.04	1.04	1.08	1.08
crystal-image plate distance (mm)	240	426	194	305
rotation/image	1°	2°	1°	2°
collimation (mm^2)	0.3 × 0.3	0.3 × 0.3	0.3 × 0.3	0.4 × 0.4
total exposure time (h)	7.0	2.0	6.5	2.5

(b) Data Collection and Processing Statistics

	TFEH	MH
cell dimensions (Å)[b]	a = 129.9; c = 104.4	a = 130.0; c = 104.3
max resolution (Å)	2.6	2.8
no. of intensities measured	66 005	125 106
no. of unique reflections	31 580	25 377
completeness (%)[c]	98.4 (96.4)	95.7 (92.4)
R_{sym} (%)[c,d]	5.1 (17.8)	7.3 (15.7)
intensity gt. 3σ (%)[c]	86.0 (64.4)	79.9 (56.2)
R to native (%)[e]	7.7	16.1

[a] Due to dynamic range limitations of the available implementation of the image plate readout system low- and high-resolution data were collected separately. The number given in parentheses is the resolution at the edge of the detector. [b] The space group is $P3_121$, so $a = b$, $\alpha = \beta = 90°$, and $\gamma = 120°$. The cell dimensions of native MADH are a = 129.8 Å and c = 104.3 Å. [c] In parentheses, the percentage in a 0.1-Å shell at the resolution limit is given. [d] $R_{sym} = \sum h[\sum i|\langle I(h)\rangle - I(h,i)|/\langle I(h)\rangle] \times 100$. [e] $R = \sum h||F_{nat}(h)| - |F_{inhibitor}(h)||/\sum h|F_{nat}(h)| \times 100$.

Synchrotron X-ray data were collected on beamlines X11(MH) and X31(TFEH) of the EMBL outstation in Hamburg (FRG) at a wavelength of 1.0 Å. In both cases, an oscillation camera equipped with a Hendrix Lentfer image plate detector was used. Due to limitations in the dynamic range (14 bits) of the available implementation of the image plate readout system, a large fraction of the reflections at low resolution usually is saturated. Therefore routinely high- and low-resolution data are collected separately. First, high-resolution data were measured with a 1° oscillation range. After increasing the crystal-to-image plate distance, low-resolution data were collected from the same crystal with an oscillation range of 2° and reduced exposure times. Details of the data collection parameters are given in Table Ia.

Data processing was carried out with the MOSFLM package (Machin et al., 1983) adapted for image plate using the profile fitting option. Corrections for absorption and radiation damage, as well as merging of low- and high-resolution data, were performed with the programs AGROVATA and ROTAVATA of the CCP4 package. The data were scaled against data of native MADH (Vellieux et al., 1990) with an overall linear scale factor and overall isotropic B factor using the program KBRANI of the Groningen Biomol crystallographic structure determination package. Data collection and processing statistics are given in Table Ib.

Prior to crystallographic refinement against the inhibitor data, the previously published model of native MADH (Vellieux et al., 1990) was refined extensively. The native diffraction data used for refinement consists of two film data sets that have been merged. One of these data sets was collected with a rotating anode source the other on synchrotron

Table II: Refinement Results

	native MADH		TFEH-inhibited		MH-inhibited	
R factor (%)[a]	20.9		18.8		18.3	
standard deviations from target values[b]						
subunit[c]	L	H	L	H	L	H
bonds (Å)	0.018	0.022	0.015	0.020	0.018	0.021
angles (deg)	3.0	3.8	2.9	3.7	2.8	3.5
contacts (Å)	0.10	0.12	0.09	0.11	0.08	0.13
rms *B* (Å^2)	3.2	3.4	3.1	3.3	3.3	3.5

[a] *R* factor is defined as $\sum||F_o|-|F_c||/|F_o|$. [b] As determined by the program TNT. [c] Separate statistics for the L and H subunit are given to show the effect of the lack of sequence information for the H subunit.

beamline X31 (Vellieux et al., 1990). Residues in the L subunit were mutated to comply with the recently determined gene sequence (Ubbink et al., 1991), and a model of the TTQ cofactor (Chen et al., 1991) was included. Water molecules were inserted at sites with a high peak in the difference electron density map and with at least one hydrogen-bond partner within 3.2 Å from the protein. Least-squares refinement was carried out with the program package TNT (Tronrud et al., 1987). The model was manually improved several times using an Evans and Sutherland PS390 system running FRODO (Jones, 1985).

For the initial assessment of changes due to inhibitor binding, SIGMAA weighted difference maps (Read, 1986) between native and inhibited MADH using phases derived from the native model were calculated. The current model of native MADH, including the cofactor atoms, but without a solvent molecule located in the active site, was used as the starting model for refinement by TNT. In the course of refinement and model building, tentative partial structures for the inhibitors comprising two nitrogen atoms were included in the model. These putative nitrogens are called "Nα", which replaces O6, and "Nβ" as depicted in Figure 2. During further refinement, Nα was restrained to the plane of the indole ring, and a bond length restraint for C6–Nα of 1.4 Å was imposed. The Nβ atom was subjected to a Nα–Nβ bond length restraint of 1.4 Å, while the C6–Nα–Nβ bond angle was unrestrained.

RESULTS

Refinement of Native MADH. The asymmetric unit contains one H and one L subunit. The present model of the L subunit contains 124 residues. No density can be seen for six N-terminal residues. The model of the H subunit comprises 373 residues whose identity due to the absence of complete sequence information is largely based upon the electron density. A total of 86 water molecules with low *B* factors have been included.

The quality of the model can be judged from the crystallographic *R* factor, which is 20.9% for data between 8.0- and 2.2-Å resolution and from the statistics on the geometry given in Table II. As expected from the lack of sequence information, the geometry of the H subunit is not as good as that of the L subunit. All main-chain ϕ,ψ combinations of residues in the L subunit are in the energetically allowed regions of the Ramachandran diagram.

There are several differences between the model of the L subunit as described by Vellieux et al. (1989) and the present model. A total of 22 residues have been mutated to comply with the gene sequence. Moreover, there are two insertions at positions 102 and 115, both located in surface loops, and one additional residue at the C-terminus. The rms difference between 121 equivalent α-carbon positions in the starting and final models is 0.44 Å. When three residues around both insertions are excluded from the comparison, this figure drops to 0.30 Å only, indicating that the overall conformation of the L subunit has not changed significantly. Because of this similarity, we will not describe the overall conformation here but instead focus on the cofactor environment.

Description of the Cofactor Environment. Figure 3 shows a close up of the cofactor and its environment. All interactions between TTQ and surrounding residues with a cutoff distance of 3.8 Å are listed in Table III. The tryptophanquinone moiety, designated as "Trq57" to indicate that it originated from a parent Trp at position 57 in the amino acid sequence, is part of a three-stranded β-sheet which consists of 16 residues and forms the core of the L subunit. One face of the indole ring is covered by a loop comprising residues 102–106 (Figure 3). The opposite side of the ring mainly interacts with Tyr74. Atoms Trq57:N1 and Trq57:O7 are within hydrogen-bonding distance of the backbone carbonyl of Ser31 and the backbone amide of Asp32, respectively, although the orientation of the latter is not optimal for hydrogen-bond formation. Atom Trq57:O6 is within hydrogen-bonding distance of Asp76:Oδ1 and Thr122:Oγ1, which both lie just below the plane of the ring. On the opposite side of the ring, O6 is hydrogen bonded to a solvent molecule located in a small pocket close to the interface of the L subunit with one of the H subunits. The wall of this pocket is made up of the side chains of residues Tyr119, Ile107, Asp32, and Asp76 and backbone atoms of residues 104–106. On one side the pocket is closed off by a residue from the H subunit. The electron density for the side chain suggests that it could be either a Phe or a His. Although this residue makes up a considerable part of the wall of the pocket, its distance to any atom of the cofactor is too long (6.5 Å) for there to be direct interactions.

Molecular surface calculations with the program MS (Connolly, 1983) using a probe radius of 1.4 Å show that the only atoms of the cofactor exposed to the pocket are Trq57:C6 and Trq57:O6. The pocket itself is not accessible from the bulk solvent, hence part of the wall of the pocket must be flexible to allow for entrance of substrate and release of products. It is not obvious what part of the wall is flexible since none of the residues surrounding the active site pocket display high *B* factors (Figure 4). The solvent molecule occupying the active site pocket has been included in the model as a water molecule, but it could also be an ammonium ion since this ion is present at a concentration of 2 M in the crystallization medium. Davidson and Jones (1992) have shown that ammonium chloride is a competitive inhibitor of MADH with a K_i of 20 mM. Preferential binding of a positively charged ammonium ion, as well as substrate recognition, may arise from the predominance of (partial) negative charges close to the active site pocket. The backbone carbonyl oxygens from three residues (Asp32, Asn104, and Ile106) as well as O6 from the cofactor are located within 4 Å of the solvent molecule. The carboxylate groups of Asp32 and Asp76 could also contribute to stabilization of a positive charge, although the short distances from Asp76:Oδ2 to Trq57:O6 (2.8 Å) and from Asp32:Oδ2 to Asn104:O (2.7 Å) indicate that both residues are protonated at pH 5, the pH used for crystallization.

The tryptophyl moiety, designated as "Trp'108" to indicate that it originated from Trp108 according to the gene sequence, points away from the pocket, pierces through the L subunit, and comes to the surface on the opposite site, exposing atoms Trp'108:C5 and Trp'108:C6 to the solvent. It has extensive

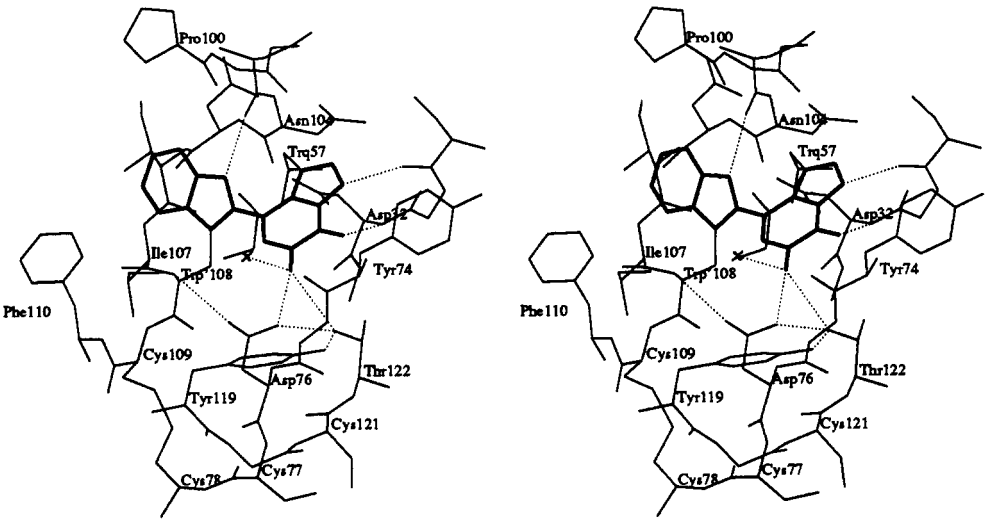

FIGURE 3: Stereopicture of the cofactor region in native MADH. Possible hydrogen bonds defined by a donor–acceptor distance shorter than 3.2 Å are indicated by dotted lines. Please note that some of the donor–acceptor orientations are not optimal for hydrogen bonding. The cross indicates a solvent molecule or ion in the active site pocket. If the structure is considered to be static, this pocket would be inaccessible to solvent. In this figure, the pocket seems accessible only since a number of residues which would block the view have been omitted.

hydrophobic interactions with residues Ile106, Phe110, and Pro100, while Trp'108:N1 is hydrogen bonded to the backbone carbonyl of Ala103.

The dynamic properties of the cofactor tryptophans, as reflected by their average *B* factors, are clearly different. The average *B* factor of the Trq57 indole atoms including the quinone oxygens is 21 Å^2, while this number is 13 Å^2 for Trp'108. For comparison, the average *B* factor of all atoms in the L subunit is 23 Å^2.

Hydrazine Inhibition. On addition of TFEH to a solution of oxidized MADH, a marked color change from green to reddish-brown was observed. The absorption maximum at 440 nm, typical of oxidized MADH, shifted to 394 nm, and a shoulder appeared around 315 nm. After removal of unreacted TFEH by dialysis, no residual enzymatic activity could be detected. The reaction with MH taking place inside a crystal could not be followed spectroscopically, but the change of crystal color was qualitatively the same as observed for TFEH inhibition in solution.

The crystals of MH- and TFEH-inhibited MADH both were isomorphous with crystals of native MADH and gave useful diffraction data out to 2.8 and 2.6 Å, respectively. Both data sets have a completeness higher than 95%. Further statistics on the diffraction data are given in Table Ib. Note that the *R* factor between the MH data and the data of native MADH of 16.1% is rather high compared with the 7.7% *R* factor between TFEH and native MADH data.

The $[F_o(\text{TFEH}) - F_o(\text{native})] \exp[i\phi_c(\text{native})]$ difference map gave a clear signal. The three highest positive peaks at 12.4σ, 11.2σ, and 8.7σ, as well as the three strongest negative peaks at 11.4σ, 5.7σ, and 5.6σ, were located close to the TTQ cofactor. All peaks outside the cofactor region were below 5.1σ.

Starting with the current model of native MADH, initial refinement against the TFEH data, consisting of 12 cycles of positional and 4 cycles of restrained *B* factor refinement, reduced the *R* factor from 20.4% to 18.9% for reflections between 8.0 and 2.6 Å resolution. When this model was inspected in $F_o - F_c$ and $2F_o - F_c$ maps, a shift of part of the cofactor and clear extra density near atom O6 of the quinone function was observed. This extra density was, quite surprisingly, by far not large enough to accommodate all atoms of the anticipated TFEH adduct. Only two atoms could be fitted into the density. For subsequent refinement, these were tentatively identified as two nitrogen atoms derived from the hydrazine (Nα and Nβ, see Figure 2). Refinement of the partial model yielded an *R* factor of 18.8% for data from 2.6 to 8.0 Å. No additional difference electron density which could possibly account for the missing trifluoroethyl moiety of the inhibitor became visible. The final model of TFEH-inhibited MADH and its electron density is shown in Figure 5B. For comparison, the model and density of native MADH, calculated at the same resolution (2.6 Å), is also shown (Figure 5A). The model for the adduct, consisting of two atoms only, nicely fills up all available density, which is clearly not coplanar with the density of the indole ring.

The difference map between MH-inhibited and native MADH contained no peaks which were significantly higher than other peaks. The highest positive and the highest negative peak in the active site region ranked 20th and 32nd, respectively. However, refinement against the MH data applying the same protocol as used for TFEH gave results similar to those obtained in the case of TFEH inhibition: (i) a shift of part of the cofactor, and (ii) clear extra density near O6 just large enought to fit two atoms, while density for three atoms had been expected. As can be seen in Figure 5C the density for MH-inhibited MADH is strikingly similar to the density obtained after TFEH inhibition shown in Figure 5B.

Conformational Changes upon Inhibitor Binding. As is clear from Figure 6, inhibition with the hydrazines only causes minor conformational changes in residues surrounding the active site pocket. There is no evidence for a widening of the pocket to provide room for the inhibitors, and the pocket remains inaccessible from the bulk solvent. As for native MADH, there is no indication of disorder in any of the residues surrounding the active site pocket. They are all well defined in the electron density and do not display high *B* factors (Figure 4).

The highest peaks present in the difference map between TFEH-inhibited and native MADH are accounted for by (i) displacement of the Trq57 indole ring (first and third positive peak and on opposite side of the ring first and third negative peak), (ii) disappearance of the solvent molecule occupying the active site pocket in native MADH (second negative peak), and (iii) extra density attached to C6 (second positive peak).

Table III: Interactions of the TTQ Cofactor of *T. versutus* Methylamine Dehydrogenase in the Native and the Two Hydrazine-Inhibited Structures[a]

		native	TFEH	MH
Trq57 atom				
N1	Ser30:O	3.0	3.1	3.2
	Tyr74:Cβ	3.5	3.5	3.5
	Tyr74:Cγ	3.5	3.6	3.6
	Tyr74:Cδ2	3.2	3.3	3.3
	Asn104:Cβ	3.3	3.3	3.3
C2	Ser30:O	3.8	3.9	3.9
	Tyr74:Cδ2	3.4	3.4	3.3
	Asn104:Cβ	3.6	3.6	3.6
C3	Ala103:O	3.5	3.6	3.6
C5	Asp76:Oδ1	3.7	3.6	3.7
	Asp76:Oδ2	3.5	4.0	4.0
	Ile106:O	3.5	3.2	3.3
	H_2O 2025	3.6		
C6	Asp76:Oδ1	4.0	3.7	3.8
	Asp76:Oδ2	3.3	3.6	3.7
	H_2O 2025	3.3		
C7	Tyr74:Cβ	3.7	4.0	4.2
C7a	Tyr74:Cβ	3.4	3.6	3.7
	Asn104:Cβ	3.6	3.5	3.5
O6/Nα[b]	Asp32:O	3.3	3.4	3.4
	Asp76:Cγ	3.5	3.5	3.6
	Asp76:Oδ1	3.4	3.0	3.1
	Asp76:Oδ2	2.8	3.1	3.3
	Thr122:Oγ1	3.1	3.5	3.6
	H_2O 2025	2.7		
O7	Ile31:Cα	3.7	4.0	4.0
	Asp32:N	3.0	3.1	3.0
	Asp32:O	3.5	3.2	3.2
	Asp32:Cα	3.8	3.7	3.6
	Asp32:Cβ	3.9	3.7	3.6
Nβ	Asp32:O		3.0	3.2
	Asp76:Oδ1		3.5	3.6
	Tyr119:Cε1		3.7	3.8
Trp′108 atom				
N1′	Ala103:O	2.9	3.0	3.0
C2′	Ile106:O	3.6	3.7	3.8
C3′	Ser56:C	3.8	3.8	3.8
C4′	Phe110:Cδ2	3.7	3.6	3.6
	Phe110:C2	3.8	3.8	3.8
C5′	Phe110:Cε2	3.7	3.7	3.7
	Phe110:Cδ2	3.8	3.8	3.8
C6′	Pro100:Cβ	3.9	3.7	3.8
	Ile106:Cδ1	3.4	3.4	3.4
C7′	Pro100:O	3.2	3.2	3.4
	Ile106:Cβ	3.8	3.9	3.8
	Ile106:Cδ1	3.4	3.4	3.4
C7a′	Ser56:O	3.8	3.8	4.0
	Ala103:O	3.7	3.8	3.8
	Ile106:Cβ	3.8	3.8	3.8

[a] Distances are given in angstroms; only distances shorter than 3.8 Å in one of the three structures are listed. [b] Atoms O6 and Nα are at equivalent positions in the structure of native and inhibited MADH, respectively.

The distance from the position occupied by the solvent molecule in native MADH and atom Nβ in the inhibited structures is about 0.8 Å.

The displacement of the modified tryptophanquinone ring can be depicted as a rotation around the C2–C3 bond. For TFEH this rotation is 5°, resulting in a shift of 0.5 Å at C6. For MH the rotation is somewhat larger: 8° and a 0.6 Å shift at C6. As a result of this shift, the angle between the planes of indoles Trq57 and Trp′108 increases from 40.0° in native MADH to 44.1° and 47.2° in TFEH- and MH-inhibited MADH, respectively. In the tentative model, only one of the atoms of the adduct (Nα) is coplanar with the indole ring of Trq57. This is reflected by a (C5–C6–Nα–Nβ) dihedral angle of −84° both for TFEH and MH.

The interactions of MH- and TFEH-inhibited TTQ with surrounding residues very much resemble those in native MADH (Table III). There are, however, some interesting differences in the hydrogen-bonding pattern. In the structure of uninhibited MADH, O6 is within hydrogen-bonding

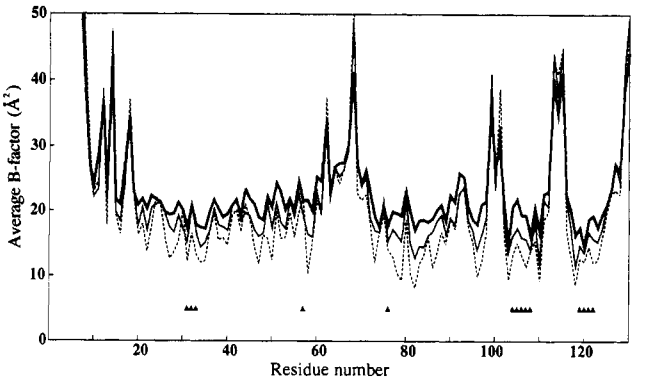

FIGURE 4: Plot of the average *B* factor values versus residue number for native (thick line), TFEH-inhibited (thin line), and MH-inhibited (broken line) MADH. Six N-terminal residues for which no electron density is observed have not been modeled. Residues close to the active site pocket are marked with triangles.

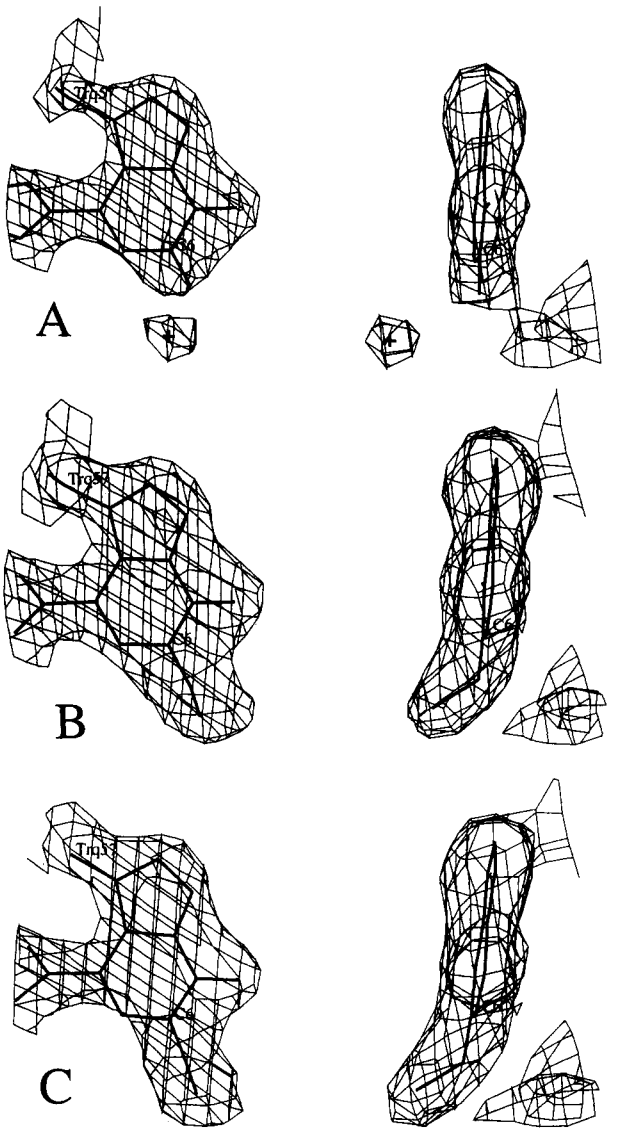

FIGURE 5: Front and side view of the models and $2F_o - F_c$ densities of (A) native MADH, (B) TFEH-inhibited MADH, and (C) MH-inhibited MADH. All maps were contoured at a level of 1σ. Both atoms attached to C6 in the inhibited structures were tentatively identified as nitrogens for the purpose of refinement and have been included in the map calculations.

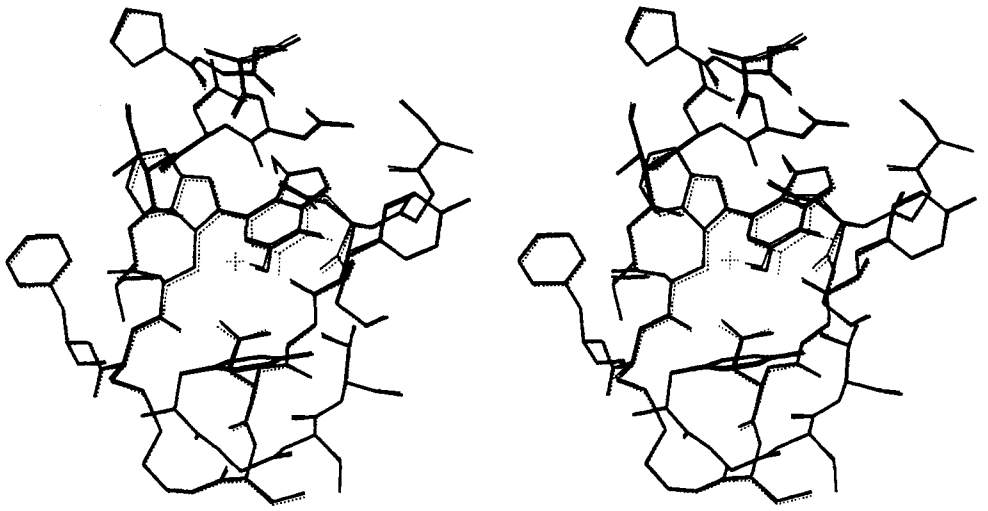

FIGURE 6: Superposition of the models of the cofactor regions of native MADH (dotted lines), TFEH-inhibited MADH (thick lines), and MH-inhibited MADH (thin lines). The cross indicates the position of a water molecule or ion in the structure of native MADH, which is absent in the models of inhibited MADH.

distance of Thr122:Oγ1 and Asp76:Oδ1. In the tentative model for hydrazine-inhibited MADH, Nα replaces O6. Due to the movement of Trq57, Nα is not within hydrogen-bonding distance of Thr122:Oγ1, their separation being 3.5 (TFEH) or 3.6 Å (MH). Instead, Nα is shifted to a position approximately at equal distances (≈3.1 Å) from both carboxylate oxygens of Asp76. As was observed for native MADH, O7 is hydrogen bonded to the backbone amide of Asp32, although the orientation is not optimal. O7 may also form a hydrogen bond, albeit a long one (3.2 Å), to the carbonyl oxygen of Asp32. Formation of this hydrogen bond would, however, only be possible if a proton is attached to O7, implicating that the cofactor may have been reduced upon inhibition.

DISCUSSION AND CONCLUSIONS

The data presented establish C6 of the TTQ cofactor of MADH as the reactive site at which nucleophilic attack takes place. This finding correlates well with the fact that, in the structure of uninhibited MADH, C6 but not C7 is exposed to the active site pocket.

Initial analysis of difference maps between native and inhibited MADH showed a much clearer signal in the active site region for TFEH than for MH-inhibited MADH. Nevertheless, partial refinement of the MADH structure against the diffraction data revealed clear extra density attached to C6 for both inhibitors. The weaker signal in the case of MH can be explained by the rather high R factor (16.1%) of these data with respect to the data of native MADH, resulting in a noisy difference map. Although many factors could be responsible for this greater difference, the actual source is not obvious. Important for this study is that the difference does not seem to arise from nonisomorphism or changes in the overall conformation of the molecule.

As mentioned earlier, the most unexpected result of our investigations is that, even though clear extra density arising from the TTQ bound inhibitors was observed, sufficient electron density was not available for either the methyl group of MH or the trifluoroethyl group of TFEH. Especially the latter had been expected to give rise to a clear signal in electron density maps.

To exclude the possibility that Wurster's blue, which was used to oxidize the cofactor, has some unexpected effect, we have determined the structure of MADH soaked only with Wurster's blue (Huizinga et al., unpublished results). A comparison of this structure with the structure of native MADH as described in this paper shows that there are no significant differences. Other causes for the lack of sufficient density could be (i) incomplete inhibition, giving rise to low occupancy, or (ii) disorder in the aliphatic parts of the inhibitors.

Since temperature factors and occupancy are correlated, high B values for the tentative Nα and Nβ atoms could be indicative of incomplete inhibition. These values are $B_{N\alpha}$ = 25 Å^2, $B_{N\beta}$ = 30 Å^2 and $B_{N\alpha}$ = 30 Å^2, and $B_{N\beta}$ = 28 Å^2 for TFEH- and MH-inhibited MADH, respectively, while the average B factors of the Trq57 indole atoms are 19 (TFEH) and 24 Å^2 (MH). The B values for TFEH are clearly above the average, but the difference is much smaller in the case of MH, making it difficult to draw firm conclusions. However, the fact that, after addition of TFEH to the protein solution and removal of excess inhibitor by dialysis, no residual enzymatic activity could be detected shows that at least in the case of TFEH all active sites have indeed reacted with hydrazine. This makes incomplete inhibition as an explanation for the lack of sufficient density improbable. Apparently, noninhibitory reduction of the cofactor to a quinol, a reaction observed between *ortho*-quinoid compounds and several hydrazines (Mure et al., 1990), does not take place significantly.

The second possible explanation for the missing density, disorder of the methyl and trifluoroethyl moieties, seems unlikely for the following reasons. Inhibition causes only minor conformational changes in residues surrounding the active site pocket (Figure 6); they remain well defined in the electron density and do not display high B factors (Figure 4). So there is no indication of disorder in the residues surrounding the pocket. Model building shows that the active site pocket can only just accommodate a methylhydrazine adduct; due to the limited space, however, it would have to pack tightly against the wall of the pocket, and the adduct is therefore not likely to be disordered. Because the active site pocket is so small, considerable conformational changes would be required to create sufficient space to accommodate all atoms of a TFEH adduct. Our data provide no evidence for such a conformational change, and therefore it seems unlikely that a complete TFEH adduct is present in the active site.

Since only two atoms could be fitted into the observed density, degradation of the inhibitors after attack of the cofactor may have taken place. We refrain from speculating about the details of this putative degradation process and emphasize that the modeling of both atoms as nitrogen should be considered tentative.

The analysis of the cofactor environment shows that TTQ is largely buried inside the L subunit, making extensive hydrophobic and hydrogen-bonding interactions. Two small patches of TTQ are solvent accessible.

The first patch, formed by C6 and O6 of Trq57, is exposed to a small pocket in the L subunit; here the reductive half-reaction takes place. It should be pointed out that the solvent molecule located in the active site pocket as well as the carboxylate moiety of Asp76 provide important information regarding the catalytic mechanism. The solvent molecule is likely to indicate the approximate position of the substrate amino group upon formation of the Michaelis complex. Due to its position in the active site pocket (Figure 3), Asp76 is almost certainly the residue responsible for proton abstraction from the α-carbon of the substrate, a step which has been proposed in the catalytic mechanism by several authors (Davidson, 1989; McWhirter & Klapper, 1989). A more detailed analysis of possible substrate-binding modes and implications for the catalytic mechanism will be published elsewhere (Huizinga et al., manuscript in preparation).

The second solvent-accessible patch, consisting of atoms C5 and C6 of the tryptophyl moiety, is located on the surface of the L subunit. A complex of MADH from *P. denitrificans* with its electron acceptor amicyanin has been crystallized (Chen et al., 1988), and the structure determination reveals that amicyanin binds close to this position (Chen et al., 1992). Hence, the tryptophyl moiety of Trp'108 is likely to be essential for electron transfer. So, clearly, the two indole moieties of TTQ have distinctly different functions in the interaction with substrate and amicyanin. The orthoquinone indole is involved in catalysis taking place in an internal cavity, while the second indole forms a crucial part of the electron transfer pathway, connecting the redox active center of the dehydrogenase with the copper center of amicyanin.

ACKNOWLEDGMENT

We thank Dr. F. M. D. Vellieux for his initial contributions to the structural studies on MADH and all members of the Groningen Protein Crystallography Group for assistance in computer programming and discussions.

REFERENCES

Backes, G., Davidson, V. L., Huitema, F., Duine, J. A., & Sanders-Loehr, J. (1991) *Biochemistry 30*, 9201–9210.

Chen, L., Lim, L. W., & Mathews, F. S. (1988) *J. Mol. Biol. 203*, 1137–1138.

Chen, L., Mathews, F. S., Davidson, V. L., Huizinga, E. G., Vellieux, F. M. D., Duine, J. A., & Hol, W. G. J. (1991) *FEBS Lett. 287*, 163–166.

Chen, L., Durley, R., Poliks, B. J., Hamada, K., Chen, Z., Mathews, F. S., Davidson, V. L., Satow, Y., Huizinga, E. G., Vellieux, F. M. D., & Hol, W. J. G. (1992) *Biochemistry 31*, 4959–4964.

Chistoserdov, A. Y., Tsygankov, Y. D., & Lidstrom, M. E. (1990) *Biochem. Biophys. Res. Commun. 172*, 211–216.

Connolly, M. L. (1983) *J. Appl. Crystallogr. 16*, 548–558.

Davidson, V. L. (1989) *Biochem. J. 261*, 107–111.

Davidson, V. L., & Jones, L. H. (1992) *Biochim. Biophys. Acta 1121*, 104–110.

de Beer, R., Duine, J. A., Frank-Jzn, J., & Large, P. G. (1980) *Biochim. Biophys. Acta 622*, 370–374.

Eady, R. R., & Large, P. J. (1971) *Biochem. J. 123*, 757–771.

Ishii, Y., Hase, T., Fukomori, Y., Matsubara, H., & Tobari, J. (1983) *J. Biochem. (Tokyo) 93*, 107–119.

Jones, T. A. (1985) *Methods Enzymol. 115*, 157–171.

Kenney, W. C., & McIntyre, W. (1983) *Biochemistry 22*, 3858–3868.

Klinman, J. P., (1991) *Curr. Opin. Struct. Biol. 1*, 968–972.

Lommen, A., Ratsma, A., Bijlsma, N., Canters, G. W., van Wielink, J. E., Frank, J., & van Beeumen, J. (1990) *Eur. J. Biochem. 192*, 653–661.

Machin, P. A., Wonacott, A. J., & Moss, D. (1983) *Daresbury Lab. News 10*, 3–9.

McIntyre, W. S., Wemmer, D. E., Chistoserdov, A., & Lidstrom, M. E. (1991a) *Science 252*, 1–7.

McIntyre, W. S., Bates, J. L., Brown, D. E., & Dooley, D. M. (1991b) *Biochemistry 30*, 125–133.

McWhirter, R. B., & Klapper, M. H. (1989) in *PQQ and Quinoproteins* (Jongejan, J. A., & Duine, J. A. Eds.) pp 259–268, Kluwer Academic Publishers, Dordrecht.

Michaelis, L., & Granich, S. (1943) *J. Am. Chem. Soc. 65*, 1747–1755.

Mure, M., Kazumi, N., Inoue, T., Itoh, S., & Ohshiro, Y. (1990) *J. Chem. Soc., Perkin Trans. 2*, 315–320.

Read, R. J. (1986) *Acta Crystallogr. A42*, 140–149.

Tronrud, D. E., ten Eyck, L. F., & Matthews, B. W. (1987) *Acta Crystallogr. A43*, 489–501.

Ubbink, M., van Kleef, M. A. G., Kleinjan, D., Hoitink, C. W. G., Huitema, F., Beintema, J. J., Duine, J. A., & Canters, G. W. (1991) *Eur. J. Biochem. 202*, 1003–1012.

van Houwelingen, T., Canters, G. W., Stobbelaar, G., Duine, J. A., Frank-Jzn, J., & Tsugita, A. (1985) *Eur. J. Biochem. 153*, 75–80.

van der Meer, R. A., Jongejan, J. A., & Duine, J. A. (1987) *FEBS Lett. 221*, 299–304.

Vellieux, F. M. D., Frank-Jzn, J., Swarte, M. B. A., Groendijk, H., Duine, J. A., Drenth, J., & Hol, W. G. J. (1986) *Eur. J. Biochem. 154*, 383–386.

Vellieux, F. M. D., Huitema, F., Groendijk, H., Kalk, K. H., Frank-Jzn, J., Jongejan, J. A., Duine, J. A., Petratos, K., Drenth, J., & Hol, W. G. J. (1989) *EMBO J. 8*, 2171–2178.

Vellieux, F. M. D., Kalk, K. H., Drenth, J., & Hol, W. G. J. (1990) *Acta Crystallogr. B46*, 806–823.